JOURNAL OF GEOPHYSICAL RESEARCH, VOL. 104, NO. A12, PAGES 28,379–28,395, DECEMBER 1, 1999

Comparison of global MHD simulations with AMIE simulations for the events of May 19-20, 1996

S. P. Slinker[1], J. A. Fedder[2], B. A. Emery[3], K. B. Baker[4], D. Lummerzheim[5], J. G. Lyon[6], and F. J. Rich[7]

Abstract.

Using WIND-measured solar wind data, we have simulated the magnetosphere for the time between 1200 UT May 19 and 0200 UT May 20, 1996, with a three-dimensional MHD model. This time period has been chosen as an International Solar-Terrestrial Physics/Global Geospace Science event for community study, and there is a large set of data with which to compare. In this paper we will compare the simulation predictions with results from the Assimilative Mapping of Ionospheric Electrodynamics (AMIE) analysis. We show comparisons for the convection, the auroral precipitation, the ionospheric conductances, the field-aligned currents, and the Joule heating distribution. The results concentrate on four time periods when the two DMSP spacecraft, F12 and F13, and the POLAR spacecraft were passing over the northern (summer) polar region. The comparisons show excellent agreement with the F13 electric field measurements. The ionospheric convection patterns agree well between the simulation and the AMIE analysis with the cross polar potential drop somewhat higher in the MHD model. The auroral electron precipitation energy flux from the MHD model is too low, particularly in the late morning, when compared with the POLAR UVI data because of the lack of electron drift physics in the model. We show how the MHD auroral input can be improved by adjusting the parameters in the auroral precipitation model.

1. Introduction

Understanding how energy is transported from the solar wind, through the magnetosphere, and into the ionosphere is becoming more important as our modern society depends on sophisticated and sensitive land- and space-based electronic systems. The geospace events on May 19 and May 20, 1996, have been chosen for special study of the energy flow by the International Solar-Terrestrial Physics/Global Geospace Science (ISTP/GGS) program. This is because of the inherently interesting solar wind stream that occurred during that time and because of the wealth of data available.

The purpose of this paper is to compare in detail the results of two fundamentally different modeling approaches to the description of the polar cap ionosphere and data from the DMSP and POLAR spacecraft. One model is a global, magnetohydrodynamics (MHD) model of the interaction of the solar wind with the Earth's magnetosphere and ionosphere. The data it uses are spacecraft-measured solar wind parameters. The model is the Fedder-Lyon model [*Fedder and Lyon*, 1987, 1995; *Fedder et al.*, 1995a, b]. The second modeling philosophy is to use all available data and incorporate it into a physically realistic model. This is the Assimilative Mapping of Ionospheric Electrodynamics (AMIE) procedure [*Richmond and Kamide*, 1988; *Richmond*, 1992]. The comparisons are made for the northern polar cap ionosphere for the time between 1700 UT on May 19 through 0200 UT on May 20, 1996. This study is the first comprehensive comparison between simulation and data for the polar ionosphere.

By its very nature, AMIE will show reasonable agreement with the measurements it assimilates, but agreement with data is by no means assured in the MHD modeling. That it occurs for this event is a major success of this study. This benchmarking of the MHD sim-

[1]Plasma Physics Division, Naval Research Laboratory, Washington, D. C.

[2]Institute for Computational Sciences and Informatics, George Mason University, Fairfax, Virginia.

[3]High Altitude Observatory, National Center for Atmospheric Research, Boulder, Colorado

[4]Applied Physics Laboratory, Johns Hopkins University, Laurel, Maryland

[5]Geophysical Institute, University of Alaska, Fairbanks, Alaska

[6]Department of Physics and Astronomy, Dartmouth College, Hanover, New Hampshire

[7]Space Vehicles Directorate,Air Force Research Laboratory, Hanscom Air Force Base, Massachusetts

Paper number 1999JA900403.
0148-0227/99/1999JA900403$09.00

ulation against AMIE and the measurements is used to improve the model and refinements have already been implemented as a result.

Only recently have the global MHD models matured enough to be compared directly with data. The most extensive comparison published to date is the Geospace Environment Modeling (GEM) Grand Challenge [*Lyons*, 1998]. During January 27-29, 1992, the Interplanetary Magnetic Field (IMF) was very strong, and there were several periods when its direction was steady. There was also good data coverage of this period. Comparisons of the global simulation models with data and with AMIE were made by several groups [*Fedder et al.*, 1998; *Raeder et al.*, 1998; *Winglee et al.*, 1997; *Lyons et al.*, 1996]. The results showed the models did well in predicting the geometry of the ionospheric convection flow patterns but tended to overestimate the strength of the electric field. The event discussed in this paper is less stressing and more typical than the GEM event, and the comparison with AMIE is given in greater detail.

The next section describes the events of late May 19 through early May 20, 1996. Section 3 briefly discusses the MHD simulation model, while Section 4 outlines the AMIE model and the data sets which were used for this study. In section 5 we give detailed comparisons of the polar cap ionosphere. We concentrate on four times when the two DMSP spacecraft, F12 and F13, were simultaneously over the pole. Section 6 summarizes the comparison for the entire period and discusses the polar cap potential drops. Conclusions are given in the final section.

2. Events of May 19-20, 1996

During this period, 1200 UT on May 19 to 0300 UT on May 20, the WIND satellite was located $\sim$ 100 R_E upstream of the Earth. Figure 1 shows the measurement of the IMF by the Magnetic Field Instrument (MFI) on WIND [*Lepping et al.*, 1995]. The plots show the field in solar magnetic (SM) coordinates which are the coordinates used in the MHD simulation. The time has been lagged by 25 min to allow for the propagation of the solar wind from the WIND position to the simulation box. Also shown are the plasma measurements made by the Solar Wind Experiment (SWE) on WIND [*Ogilvie et al.*, 1995]. The data in Figure 1, except for B_x, are input to the front boundary of the MHD simulation. The vertical lines show times that the DMSP spacecraft are both over the northern polar cap. The POLAR satellite was above the northern polar region throughout this period.

During this event the solar wind speed and density were fairly steady. The IMF was weakly northward until a little after 1900 UT, when it turned weakly southward for about an hour. The northern aurora were very dim until a brightening and small substorm occurred at 2020 UT, localized in the premidnight sector. The aurora became less active again until after midnight at the onset of a second substorm. This resulted from the steady southward IMF which began at 2100 UT. B_y was dawnward during the early part of this event but had several significant duskward and dawnward fluctuations later. The response of magnetosphere to these IMF conditions during the early part of this period has been discussed previously along with comparisons of the simulation results with POLAR magnetic field measurements [*Fedder et al.*, 1997].

3. MHD Model Description

The simulation model solves the equations of MHD. Details on the model equations and the numerical techniques used to solve them can be found in the works of *Fedder and Lyon* [1987, 1995], *Fedder et al.* [1995a, b], and *Mobarry et al.* [1996]. The model is three dimensional with a nonuniform, distorted spherical grid. The X axis is perpendicular to the Earth's magnetic dipole axis. The grid extends roughly 24 R_E sunward of the Earth to $X \sim$ -300 R_E tailward and 90 R_E in the lateral Y and Z directions, with Z along the northern dipole axis and Y positive to the duskward direction. The simulation coordinate system is the same as the solar magnetic, SM, system. The grid is a distorted spherical mesh which has 50 cells in the "radial" direction and is 48x64 in the angular directions. There is an inner boundary in the interior of the grid which is a spherical region with a radius of $\sim$ 3.2 R_E centered on the Earth. Field-aligned currents (FACs), calculated in the magnetospheric grid, are mapped from this boundary to the ionosphere where they are the source for the polar cap potential. The potential equation includes both Pedersen and Hall conductances. The solution for the potential provides an electric field which is mapped back to the inner boundary of the magnetospheric grid where it is used as a line-tying boundary condition for the MHD solution.

The basic equation for the potential Φ solved in the ionosphere is

$$\nabla \cdot \overline{\Sigma} \cdot \nabla \Phi = J_{\parallel}, \tag{1}$$

where $\overline{\Sigma}$ is the ionospheric height-integrated conductance tensor and $J_{\parallel}$ is the current parallel to the field line which is mapped from the magnetosphere. Our conductance tensor has two parts: a solar EUV conductance and an auroral precipitation-enhanced conductance. The solar contribution depends on the observed solar radio flux at 10.7 cm and the zenith angle. In our model the seasonal and diurnal variations of the magnetic dipole are taken into account. The solar contribution to the Pedersen and Hall conductances come from a fit to incoherent scatter radar data (H. Kroehl, private communication, 1990). For this run the solar $F_{10.7}$ flux was taken as 70, which gave Pedersen conductances on the dayside 60° magnetic latitude line of $\sim$ 7 Siemens in the summer hemisphere and 3 Siemens in the winter.

The auroral contribution to the ionospheric conductance involves estimating a precipitating electron energy flux and a "typical" energy, including effects due to field-aligned potential drops, and then using the data

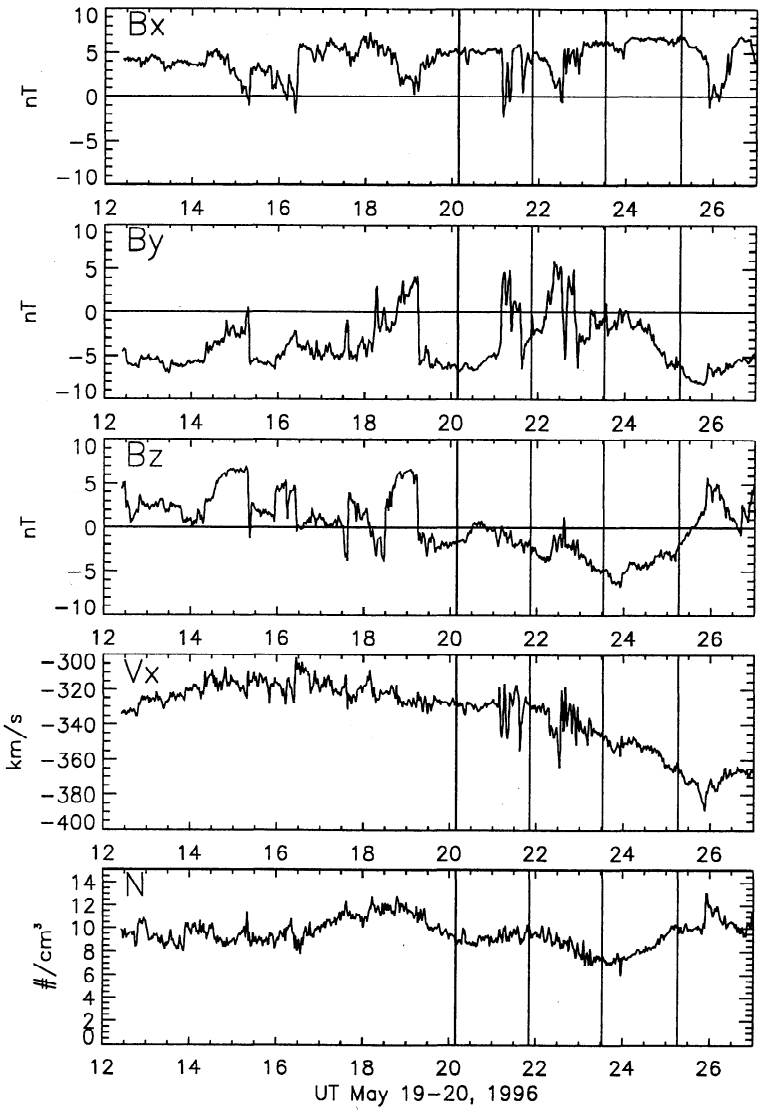

Figure 1. Solar wind measurements by WIND [*Lepping et al.*, 1995, *Ogilvie et al.*, 1995] during the event. The data were rotated to the solar magnetic (SM) system and delayed by 25 min to account for propagation time to the Earth. These data, except for B_x, are directly input to the simulation. The four vertical lines indicate times when the DMSP spacecraft were over the northern polar cap.

fits of *Robinson et al.* [1987], to estimate the conductances. The precipitating electron energy flux is the product of the typical or average energy E and the particle flux Ψ. These quantities are found in a two-step process. The first step is an initial estimate based on the magnetospheric plasma at the inner boundary of the simulation. The second step includes the effects of field-aligned potential drops and magnetic mirror physics to improve the initial estimates. One of the purposes of doing real event modeling is to compare ionospheric measurements with the simulation in order to improve the auroral precipitation model.

The initial energy and particle flux estimates are found from

$$E_0 = \alpha c_s^2, \tag{2}$$

$$\Psi_0 = \beta \rho E_0^{1/2}, \tag{3}$$

where c_s and ρ are the sound speed and the plasma density taken from the inner boundary of the MHD grid. Here α and β are parameters which are chosen by benchmarking simulation results with observations. Their values are fixed, both spatially and in time, for each simulation run. They were originally set by comparing with auroral images from VIKING [*Fedder et al.*, 1995b] and revised in comparison with ionospheric simulations (J. Sojka, M. Bowline, and R. Schunk, private communication, 1996). As a result of this event, we will adjust β by a factor of 2.56.

In the second step of the calculation the energy gained in the field-aligned potential drop $E_\parallel$ along the dipole field line between the inner boundary of the magnetosphere grid and its foot point in the ionosphere is given by

$$E_\parallel = R J_\parallel E_0^{1/2}/\rho, \tag{4}$$

where R is an adjustable scaling factor for the potential drop and includes an "effective resistivity" to FACs. The factor R is chosen to be 5 times larger for current out of the ionosphere as opposed to current into the ionosphere. R is fixed in the model but may be adjusted in the future as more comparisons with data are made. Equation (4) is based on work of *Chiu and Cornwall* [1980] and *Chiu et al.* [1981].

Finally, the calculation adjusts E_0 and Ψ_0 for the effects of the field-aligned potential drops in the geomagnetic mirror field configuration. Following *Orens and Fedder* [1978],

$$\Psi = \Psi_0(8 - 7exp[-E_\parallel/(7E_0)]) \qquad E_\parallel > 0, \quad (5)$$

$$\Psi = \Psi_0 exp[E_\parallel/E_0] \qquad E_\parallel < 0, \quad (6)$$

$$E = E_0 + E_\parallel. \quad (7)$$

The model discussed by *Robinson et al.* [1987] is then used to get the auroral contribution to the ionospheric conductance,

$$\delta\Sigma_P = 2.5E(E\Psi)^{1/2}/(1 + 0.0625E^2) \quad (8)$$

$$\delta\Sigma_H = 0.45E^{0.85}\delta\Sigma_P, \quad (9)$$

where $\delta\Sigma_P$ and $\delta\Sigma_H$ are the Pedersen and Hall conductances in Siemens when E is in keV and $E\Psi$ is in mW m^{-2}. The auroral conductances are combined with the solar radiation conductances as the square root of the sum of the squares.

The simulation is run by specifying the solar wind and IMF conditions at the sunward side of the grid. The parameters used as input are the plasma density, plasma sound speed, the three components of the velocity, and the Y and Z components (in the SM system) of the IMF. All of these input conditions are assumed to be independent of Y and Z. B_x is set to zero in order that the magnetic field entering the simulation box is divergenceless. For this event the measurement of the solar wind by the WIND spacecraft as shown in Figure 1 was used.

The initial condition of the magnetosphere at the beginning of the simulation was chosen from a database which contains many previous runs. We choose a magnetospheric configuration which we expect to be approximately correct. Preliminary runs are made to make a transition to a more accurate initial state of the magnetosphere as can be best guessed. Once the simulation begins the dayside magnetosphere approaches the actual situation within 10 to 20 min, whereas the proper state of the magnetotail takes longer to develop, depending on how close the initial conditions were to the real state of the tail.

4. AMIE Model

The Assimilative Mapping of Ionospheric Electrodynamics (AMIE) procedure combines statistical models and data in four separate least square fitting solutions to find [*Richmond,* 1992; *Emery et al.*, 1996]: 1) the auroral energy flux, 2) the average auroral electron energy, 3) the Pedersen and Hall height-integrated conductances, and 4) the electric potential, currents, and other electrodynamics.

The May 19-20, 1996, study used values of the auroral energy flux and mean energy derived from two N_2 Lyman-Birge-Hopfield (LBH) filters on the UltraViolet Imager (UVI) aboard the POLAR satellite [*Torr et al.*, 1995; *Germany et al.*, 1997; *Lummerzheim et al.*, 1997]. The sunlight emissions were removed, resulting in images of the entire auroral oval about every 5 min in the northern hemisphere. The Pedersen and Hall conductances were then found in an analogous manner to *Lummerzheim et al.* [1991] from the UVI estimates of the auroral energy flux and average energy, adopting the updated model results from *Rees et al.* [1995]. Therefore it was unneccessary to find least square fits to (1)-(3) using sparser data sets and statistical models, and the only solution found was for the electric potential and currents, using the given auroral information from UVI on POLAR. The statistical electric potential model used was the *Weimer* [1995, 1996] model based on season (dipole tilt), IMF (B_y and B_z), and the solar wind velocity. The electric and deviation magnetic field data sources used were the following: 1) 95 ground magnetometers (85 in the northern hemisphere), 2) DMSP-F12 and F13 Ion Drift Meter (IDM) ion drifts perpendicular to the satellite track, 3) Six northern hemisphere SuperDARN HF radars with ion drift velocities, and 4) Sondrestrom IS radar ion drifts.

Solutions were found for the four times of the northern hemisphere DMSP overpasses using data averaged over 26 min. Different patterns were found using data averaged over 5 minutes for 115 POLAR UVI images between 1705 UT on May 19 and 0303 UT on May 20. With the large amount of data, the initial electric potential patterns were not very important to the final results.

5. Comparisons During DMSP Spacecraft Passes

The DMSP spacecraft, F12 and F13, were recording plasma convection and electron precipitation during this time [*Rich et al.*, 1987]. These spacecraft are in polar orbits at altitudes of around 800-900 km and take 20-25 min to pass over the high-latitude polar regions. There were four times during this period, ~ 2009, 2151, and 2332 UT on May 19 and 0116 UT on May 20 when both satellites were simultaneously over the northern polar cap. DMSP data are routinely assimilated into the AMIE procedure. At these four times, detailed comparisons between the AMIE and MHD simulations will be shown in this section.

The MHD model covers both the northern and southern polar ionospheres, while AMIE can model either one or both depending on the availability of the data. For May 1996 the solar $F_{10.7}$ output was low (we used 70 in the MHD simulation), so the amount of He^+ was increased in the winter pole, making the DMSP ion drift

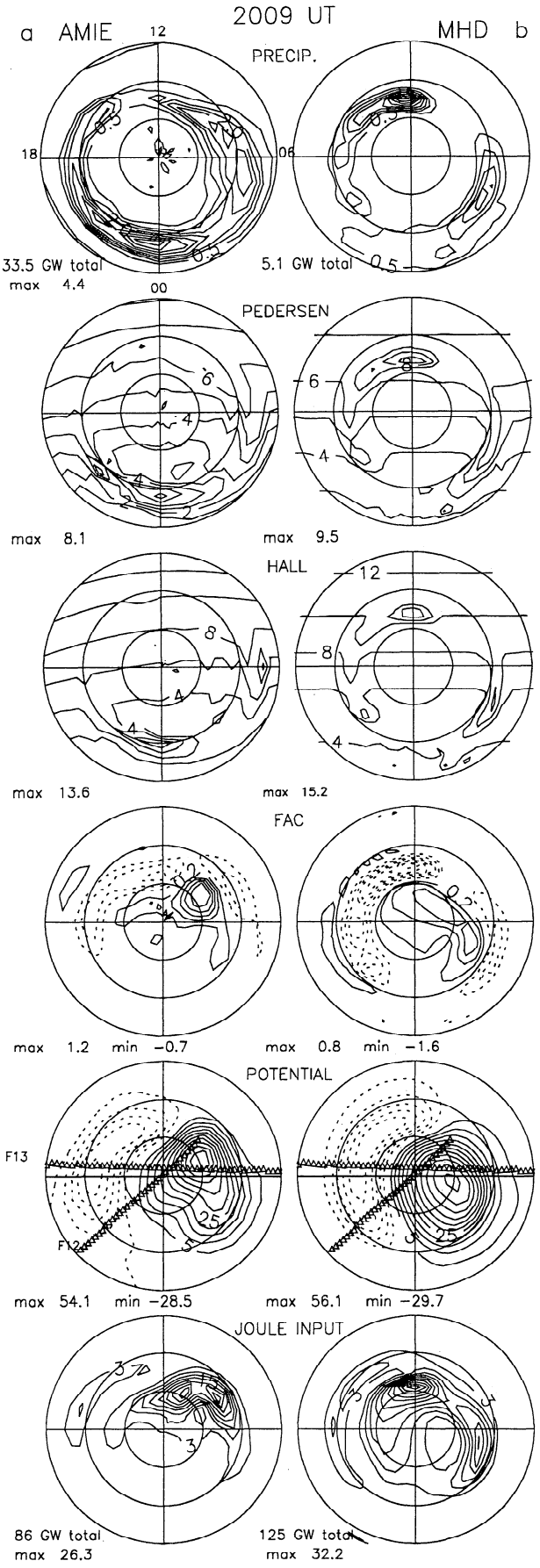

measurements difficult there, and so comparisons were not made for the southern hemisphere passes for this event.

5.1. Synoptic Maps

Figures 2-5 give detailed comparisons between the MHD simulation and the POLAR UVI data and AMIE simulation for the four times when F12 and F13 were over the northern polar region. Figure 2 shows the northern polar cap at 2009 UT. Figure 2a gives the UVI/AMIE result, and Figure 2b gives the MHD simulation result. The plots are centered on the magnetic pole and circles are drawn every 10° in magnetic latitude down to 60°. The AMIE simulation provides results to 44° magnetic latitude while the lower limit of the MHD model is about 58°. In these plots, noon is at the top, and dawn to the right.

The first row of Figure 2 plots contours of the precipitating energy input to the ionosphere. The AMIE result is the averaged data that was derived from the UVI measurement. The total power into the northern polar cap is 33.5 GW. The MHD simulation result was 5.1 GW. For the MHD contour plot we have multiplied the intensity in the MHD results by 2.56, rather than use different contour levels, so that more contours are seen. The total power of 5.1 GW was not scaled. The model described in section 3 for the ionospheric precipitation in the MHD simulation gives a total hemispheric power input to the ionosphere from precipitating electrons much lower than that inferred from the UVI measurements throughout this event. Part of the purpose of this study is to adjust the MHD model to get better agreement with measurement, and in fact, we have chosen to increase the factor β in eq. (3) by 2.56 in future simulations. This multiplies the auroral Pedersen conductance by a factor of 1.6.

Figure 2. Comparison of northern polar cap quantities between the (a) AMIE model and the (b) MHD simulation at 2009 UT. Noon is at the top, and dawn is to the right in each polar plot. The north magnetic pole is at the center and latitude circles are drawn every 10°. The first row shows contours of the precipitating electron energy flux with contour levels at 0.5 mW m^{-2}. The AMIE result is the averaged UVI measurement. The contours (but not the total) for the MHD result have been multiplied by 2.56. The second row gives the Pedersen conductance with contour levels 1 Siemens. The third row is the Hall conductance with contour levels 2 Siemens. The fourth row gives contours of the field-aligned currents with contour levels of 2 μA m^{-2} and upward current (negative values) dashed. The zero contour is not drawn. The fifth row is the polar cap potential with contours every 5 kV and the 0 contour not drawn. The trajectories of F12 and F13 are shown with the spacecraft traveling from left to right. Only the part of the F12 orbit is shown for which data was used. The last row give contours of the Joule energy deposition rate with 3 mW m^{-2} levels.

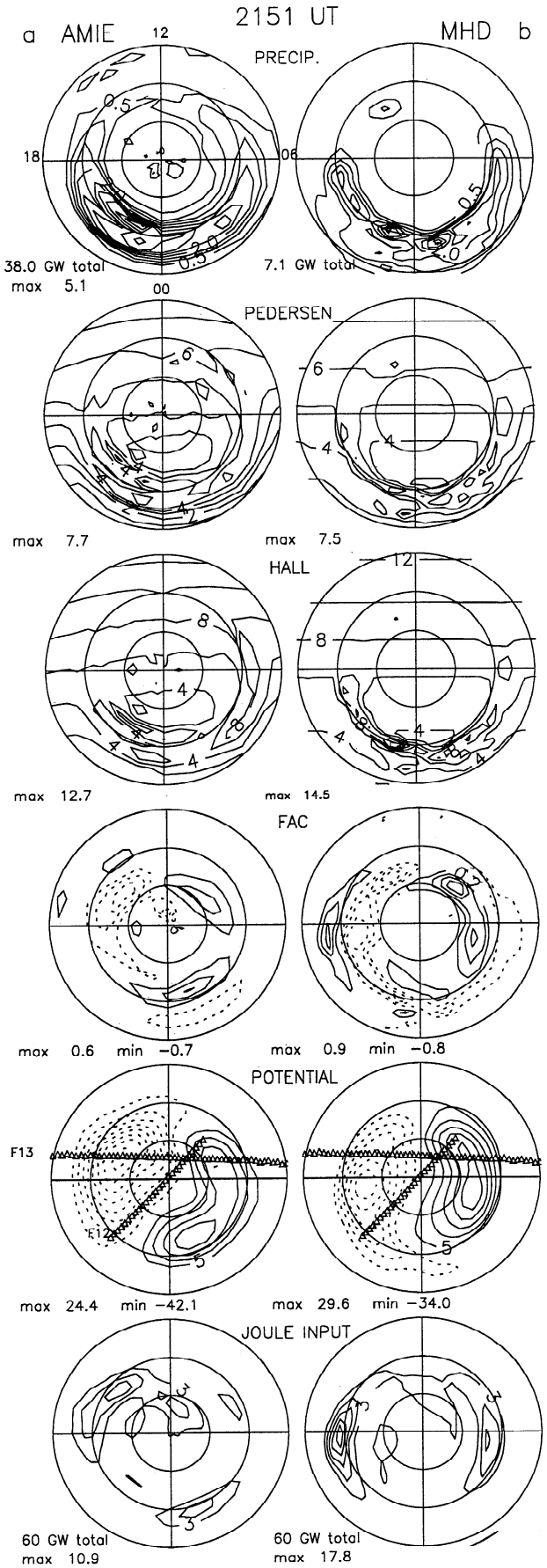

In the MHD model, once the precipitation is known, the fits of *Robinson et al.* [1987] (equations (8) and (9)) give the auroral enhancement to the ionospheric conductance. For AMIE, the results of *Rees et al.* [1995] are used. Combining this with the solar EUV contribution, the Pedersen and Hall height-integrated conductances are found. These are displayed in rows 2 and 3 of Figure 2.

The second row shows contours of the height-integrated Pedersen conductance in the ionosphere, with levels drawn every Siemens and every even value labeled. The third row gives the Hall conductance with levels every two Siemens. Dayside conductance is dominated by the solar EUV contribution so both models agree fairly well there. Both models show enhanced conductance along the auroral oval, with morning side enhancements agreeing well. The evening enhancement in the oval is somewhat higher in the MHD simulation. Both models have the morning oval at slightly lower latitude than the evening oval. The most striking differences in conductances occur at noon and midnight. The MHD simulation shows a much stronger conductance feature at noon where there is an extension of the upward Region 1 current across noon due to the negative B_y in the solar wind. This current is also deduced from AMIE but at a weaker magnitude (see the fourth row of Figure 2). Both F12 and F13 just miss this region. However, we feel the MHD model tends to overestimate the conductance here. The reason is that the model assumes a single ratio of the electron temperature to the ion temperature. (This is related to the spatial constancy of the model parameter α in equation (2)). That number was benchmarked against data in the midnight regions where the plasma sheet plasma is hotter than the cusp/cleft plasma which precipitates on the dayside.

The second major disagreement is the enhanced conductance seen in the UVI/AMIE plots a little before midnight. For reasons we do not understand, the MHD simulation did not reproduce this auroral activity in the northern hemisphere, although substorm activity was occurring in the south.

Note that the differences between the two models in the Pedersen conductance are not as great as might be expected from the difference in total precipitating power shown in the first row. If the average energies are comparable, then eq. (8) shows that the Pedersen conductance scales with the square root of the energy flux. In addition, the dayside is dominated by the solar contribution. For a given energy and energy flux, the Pedersen conductance in the *Rees et al.* [1995] for-

Figure 3. Comparison of AMIE and MHD results at 2151 UT. The format and contour levels are the same as Figure 2. The contours of precipitating electron energy flux for the MHD result have been multiplied by 2.56.

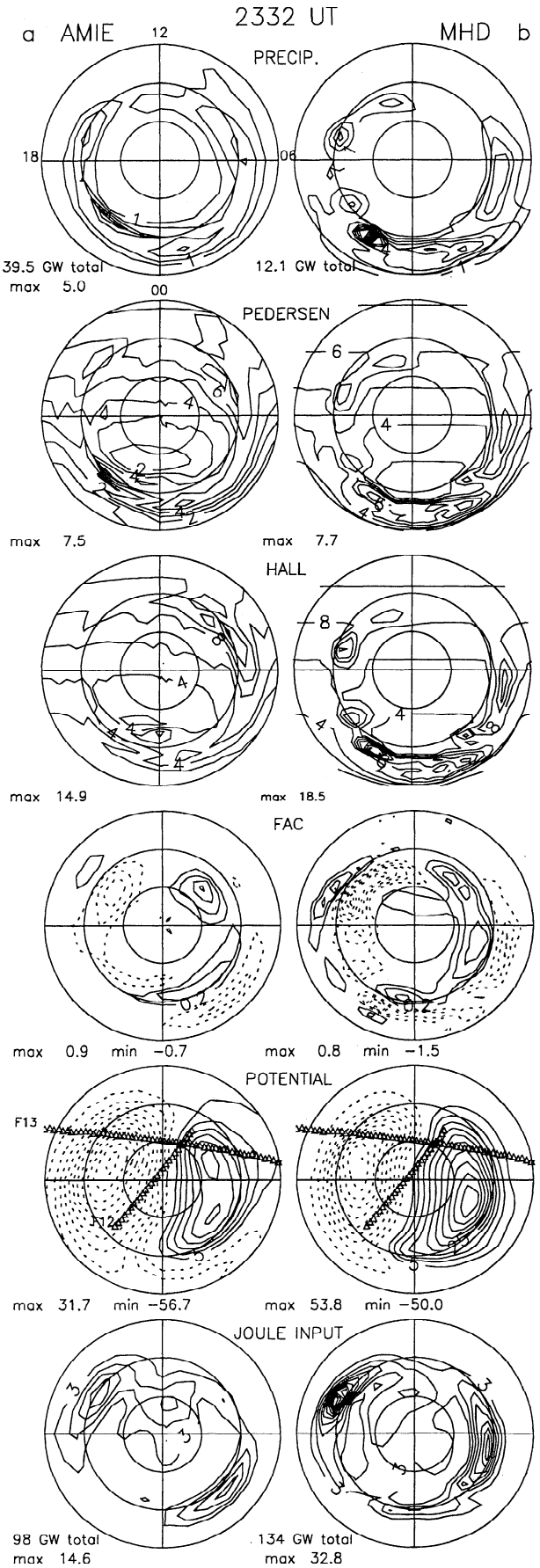

mulation used in AMIE is somewhat higher, typically 20%, than the *Robinson et al.* [1987] result used in the MHD model. For this reason, we have chosen to increase the conductance by 60%, using an enhanced factor of f=2.56 for the electron flux. This will bring the conductances in AMIE and the MHD closer, but the MHD precipitating power will still be low. Future event studies will be used to reconcile the differences between the simulation models, the conductance models, and the measurements.

The fourth row of Figure 2 gives the FACs for the two models with upward current contours dotted. Both results show the upward Region 1 system extending across noon into the morningside, typical of a negative IMF B_y. The dawn downward current is more concentrated in the AMIE result and more to the dayside, consistent with the potential patterns. Region 2 currents are slightly stronger in the MHD results, with the dawn Region 2 shifted to the nightside.

The FACs are the most fundamental quantities in the model of the ionosphere in the MHD simulation in that the other quantities depend on them, and the FAC systems extend out into the magnetosphere and are generated there. In contrast, in the AMIE formulation, the FACs are one of the most derived quantities. AMIE uses the precipitation to determine the conductances and then the magnetometer, radar, and DMSP measurements to obtain the horizontal ionospheric currents. The FACs can then be found assuming that the total current density is divergenceless.

The fifth row shows the polar cap potentials with the F12 and F13 orbits superimposed. The F12 orbit shows only the part of the trajectory for which data was used. The total potential drop, geometric shapes of the convection pattern, and electric fields along the spacecraft trajectories agree between the simulations. The crescent-circular two-cell patterns result from the negative B_y of the IMF. AMIE shows the center of the dawn cell slightly to the dayside of the F13 path, while the MHD model has it slightly nightward. For the MHD model, the potential is found from eq. (1). For AMIE, the horizontal ionospheric current systems inferred from the magnetometers, the electric fields from DMSP, and the ion convection measured by the radars, combined with the conductance, are used to find the potential.

Again, the agreement in the models might be surprising given the difference in precipitation reflected in row 1 of Figure 2. However, the main potential drop is across the dayside where the solar conductance dominates.

The sixth row shows contours of the expected Joule heating input to the ionosphere with contours drawn

Figure 4. Comparison of AMIE and MHD results at 2332 UT. The format and contour levels are the same as Figure 2. The contours of precipitating electron energy flux for the MHD result have been multiplied by 2.56.

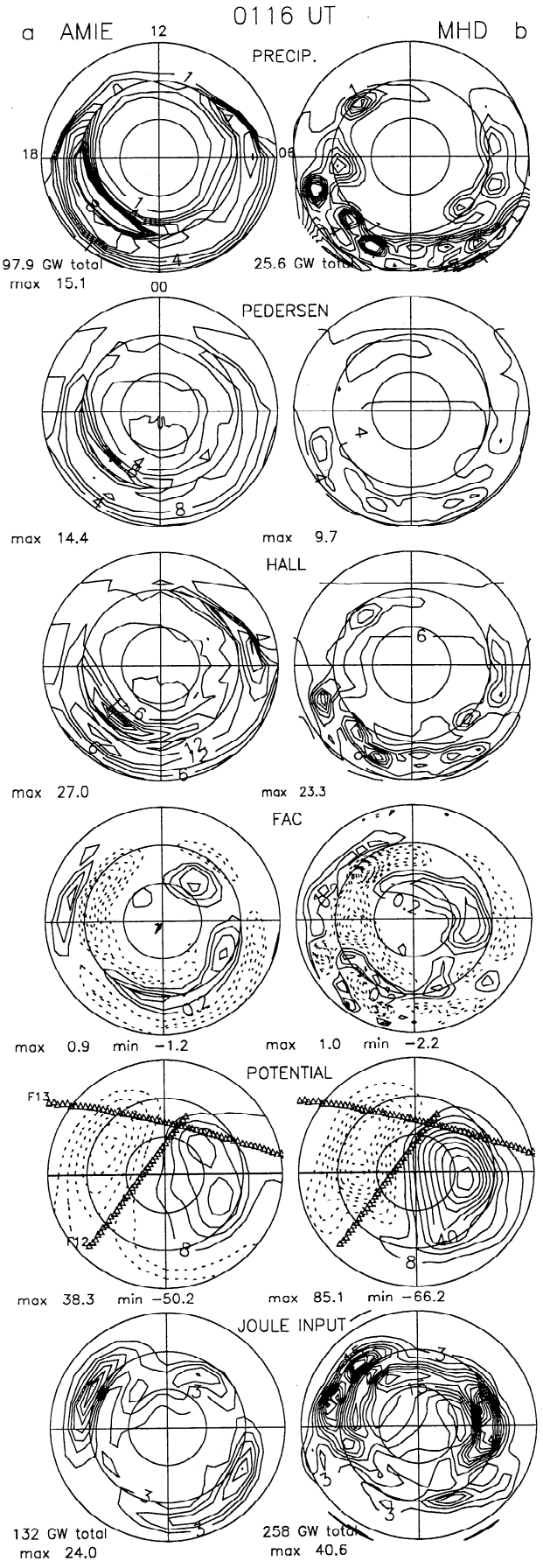

every 3 mW m^{-2}. Both models show three regions of heating: the weakest one along the evening auroral oval at $\sim 70°$, a second along the dawn oval, and a third extending longitudinally at $\sim 80°$ across the dayside. The most intense Joule heating occurs on the dayside. This quantity is a derived quantity in both models.

Figure 3 shows the same quantities with the same contour levels as Figure 2, but at 2151 UT, the next time F12 and F13 pass over the northern polar cap. The IMF B_z has remained near 0, while B_y, after holding near -5 nT, has swung duskward and is also small.

The geometric distribution of auroral precipitation agrees fairly well between the two models, with UVI/AMIE producing more along the morning oval. The MHD result is about a factor of 5 lower in total hemispheric power input.

The conductances from the two models agree better than at the previous time. Both show the largest enhancements in the premidnight sector at $\sim 70°$ magnetic latitude. The dayside hotspot has disappeared from the MHD result.

The FACs have weakened. Both models now show current wedge systems near midnight which were not there at 2009 UT. The AMIE currents are postmidnight while the MHD currents are most intense premidnight. Again, the MHD model shows stronger Region 2 systems.

Because the strength of the IMF has dropped, the total cross polar potential is less. Both models show about the same value. The potential structures seen along the F13 path are very similar. The MHD pattern for F12 is more structured than the AMIE pattern in the premidnight sector, showing a greater influence of the auroral enhancement there. The AMIE patterns are more skewed in the clockwise direction showing a stronger IMF B_y effect.

The Joule heating rate has decreased with the most intensity along the afternoon oval. AMIE sees stronger heating at midnight, while the MHD simulation has more along the morning oval.

The next DMSP transits occurred near 2332 UT and the simulation results are compared in Figure 4. UVI/AMIE gives more intense auroral precipitation input in the dayside dawn oval. Both models show strongest input near 70°, 2100-2200 MLT, and also at 1700 MLT. The total power is about a factor of 3 lower

Figure 5. Comparison of AMIE and MHD results at 0116 UT. Since the ionosphere is more active at this time the contour levels have changed in some of the plots. The contour levels for the precipitating electron energy flux (row 1) are 1 mW m^{-2}; for the Pedersen conductance (row 2) they are 2 Siemens; for the Hall conductance (row 3) they are 3 Siemens; and for the potential (row 5) they are 8 kV. The contours of precipitating electron energy flux for the MHD result have been multiplied by 2.56.

in the MHD simulation. The most striking difference in the conductances occurs along the dusk oval, where the MHD shows some intensifications which are especially strong in the Hall conductance. Both models show the dawnside oval at slightly lower latitude than the duskside.

The MHD FAC patterns again show more structure and stronger Region 2 systems than the AMIE patterns. In the premidnight sector the MHD result shows current pairs where the auroral enhancements are located.

The IMF B_z has remain southward and has strengthened somewhat resulting in a greater potential drop. B_y has oscillated around zero and the patterns are fairly symmetric between dawn and dusk. The MHD result has a stronger dawn cell, but the potential fields along the DMSP paths are similar in both models. Geometrically, the Joule heating patterns agree between the simulations, with the MHD showing stronger deposition and morningside heating more sunward. The total hemispheric power input due to Joule heating is ~ 1.3 times higher for the MHD simulation at this time.

The IMF remained southward and a substorm occurred after midnight. The ionosphere is still in a disturbed state by the time of the next DMSP transit around 0116 UT as shown in Figure 5. For this last figure we have changed some of the contour levels from the previous three figures but still keep the AMIE and MHD contour levels the same, remembering that the MHD auroral precipitation levels have been multiplied by 2.56.

The greatest conductance enhancements occur in the late evening sector, with the UVI/AMIE result slightly stronger and at a higher latitude. UVI/AMIE shows much more activity in the dawnside oval at late morning, while the MHD model has an intense spot in the afternoon. The FACs are stronger than at the previous times with the MHD result more structured than the AMIE output. Both models show a downward current sheet in the premidnight sector where the most intense activity is.

The MHD model has a larger potential drop mainly because of the stronger positive potential cell in a region where the AMIE analysis does not have data. The potential structures along the F13 orbit are very similar. The MHD result shows the dusk cell extending across the F12 path around 75° in the late evening which is not as pronounced in AMIE, however, there may be indications of a small signal at F12 there (see Figure 6a, bottom, at 1.1 UT below).

As a result of the higher potential drops, the Joule deposition is stronger, by a factor of 2, in the MHD result, both models giving the most intensity around 65° in the midafternoon. There is also midafternoon auroral precipitation. Again, the MHD simulation does not show late morning intense precipitation probably because of the lack of electron drift physics in the model. We are currently investigating ways to account for this in the MHD code. The MHD precipitation power is a about a factor of 4 lower at this time.

5.2. Electric Fields

Figure 6 shows the electric field along the spacecraft track for F12 and F13. F12 traveled from around 2100 MLT to 1000 MLT and F13 from dusk to dawn on the dayside of the terminator. The spacecraft measures the ion velocity distribution perpendicular to the path. The convection velocity is derived and then mapped to 110 km altitude where it is converted to the electric field along the orbit. The data are averaged over 20 s and any offsets are removed. The electric field is then used in AMIE. In Figure 6a the F12 electric field is shown as a solid line. The value which AMIE returns after the measurement is assimilated with all the other input is shown as a dashed line. The value derived from the MHD simulation is dotted. The time step in the MHD simulation is a fraction of a second, but for these plots, we have picked a fixed time in the middle of the spacecraft overpasses and calculated the field along the entire orbit path. These times are shown in Figures 2-5. During periods when conditions change rapidly compared to the 20-min orbit crossing time, this comparison could be improved by resolving the simulation electric fields more frequently. This would produce only minor improvements for this event. Figure 6b shows the electric field for F13.

Agreement of the MHD simulation with F13 electric field data is much better than with F12. The signal on F13 is much cleaner, whereas F12 moves from darkness to the sunlight making the measurement more difficult. Moreover, Figures 2-5 show that F13 passes near the peaks of the two ionospheric convection cells, while F12 passes between the cells.

5.3. Precipitation Measurements

Figures 7a and 7b show the precipitating electron energy flux. The solid line shows data from F12 and F13 taken every 15 s. The dashed line shows the precipitating electron energy flux from the UVI measurements which were averaged spatially over 2 deg of latitude and 1 hour of MLT. The UVI measurements were averaged over 25 min. The dotted line gives the MHD simulation result. We have multiplied the simulation result by 2.56, so that it can be seen on the same scale. Geometrically, the curves match up fairly well showing that the simulation is predicting the position of the auroral oval accurately. Even with the enhancement factor, which will be incorporated in future simulations, the morning precipitation is too low in the model. However, this is not surprising as the electrons move to the dayside around the dawn by drifts which are not described in the ideal MHD formulation. The UVI and DMSP measurements agree well, with the UVI flux somewhat stronger and broader. The broader fluxes are due to spatial averaging in the UVI data, while the temporal averaging favored higher flux measurements. The data for the second pass of F12 were discussed by *Germany et al.* [1997].

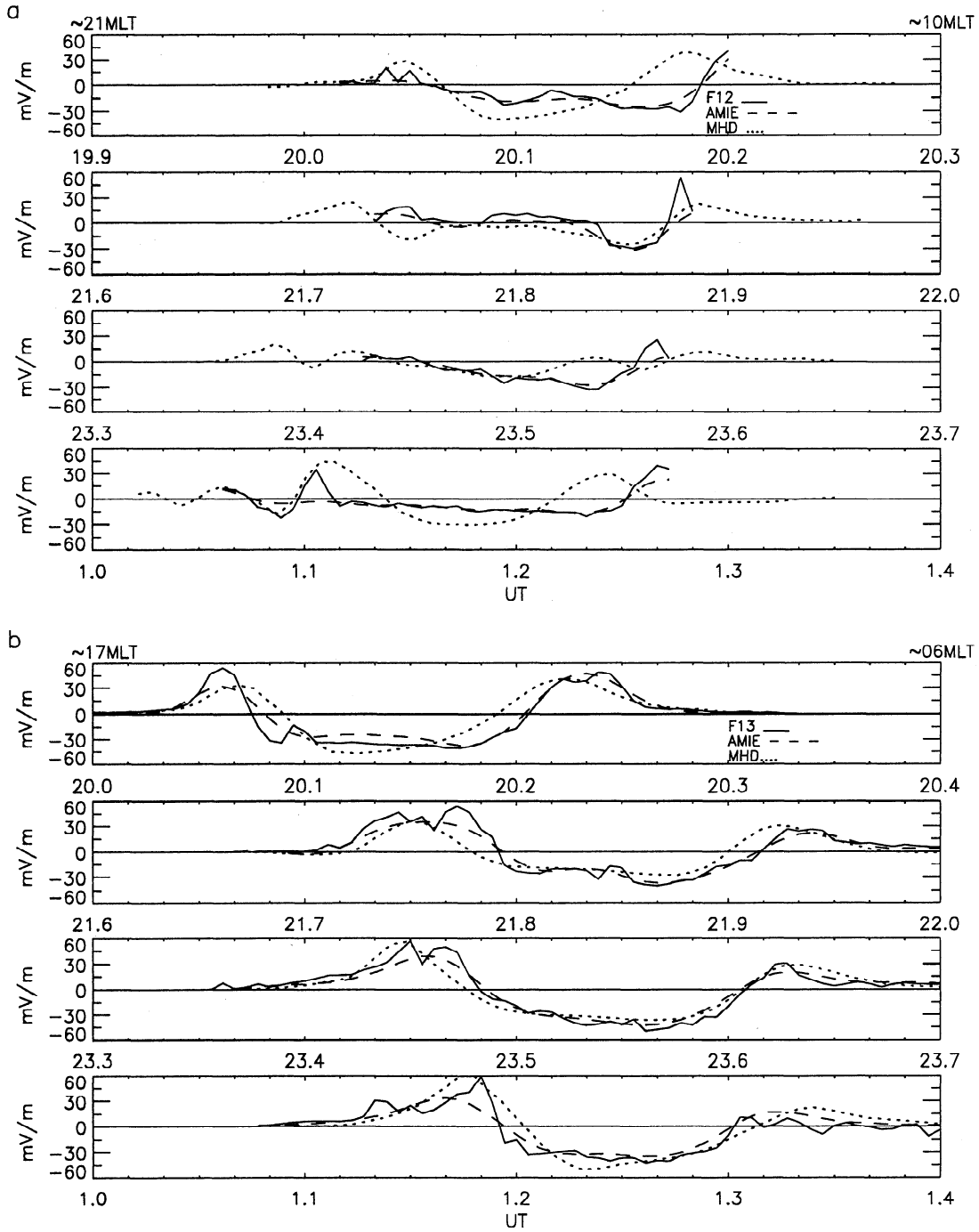

Figure 6. (a) The electric field along the F12 trajectories over the north pole for the four overpasses during this event. The solid line gives the measurement. The dashed line is the AMIE result, and the dotted line gives the MHD simulation prediction. The spacecraft trajectories are shown in Figures 2-5. (b) The electric field along the F13 trajectories.

Differences between the DMSP- and UVI-derived energy flux and average energy are due to different inherent spatial and temporal resolution of the measurements. DMSP makes a 1 s (~ 7 km) average along a one-dimensional track, while UVI image pixels are two-dimensional spatial averages over a 37-s integration time. In the subsequent analysis of the images, many pixels are averaged together to obtain spatial averages on a grid of 2 deg of latitude and 1 hour of MLT. The DMSP data are averaged over a comparable time but remain a one-dimensional cut through the two-dimensional image.

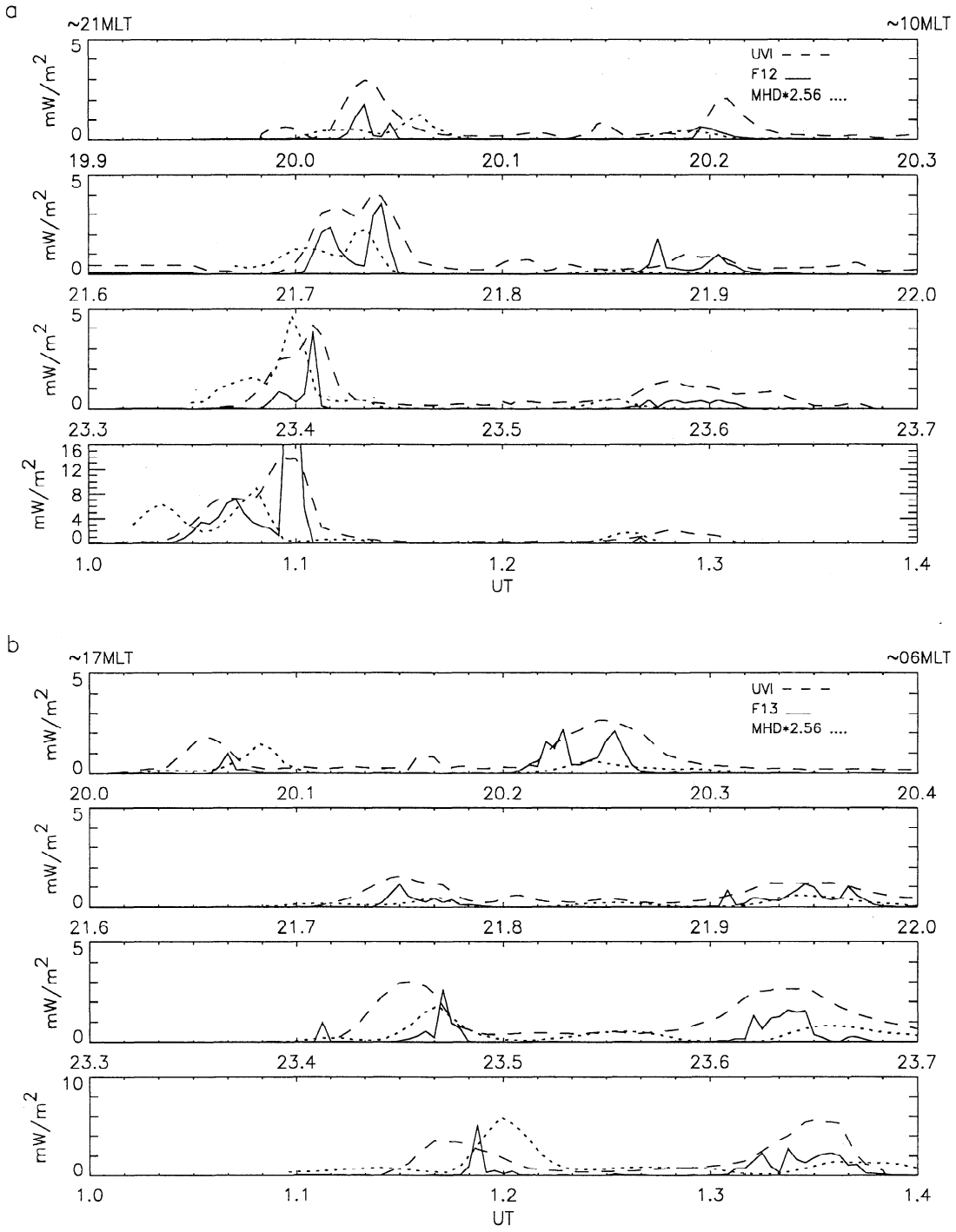

Figure 7. (a) The precipitating electron energy flux measured by F12 (solid), measured by the UVI (dashed), and predicted by the MHD simulation (dotted). The MHD results were multiplied by 2.56 so they could be seen. (b) The precipitating electron energy flux seen by F13.

Figures 8a and 8b show the average energy measured by the DMSP spacecraft and the UVI along with that predicted by the simulation. This number is difficult to infer from the precipitation measurements. The DMSP average energy is computed from the ratio of the electron energy flux to the number flux using energies between 460 eV and 30 keV [*Rich et al.*, 1987.] The UVI average energy is computed using the technique described by *Lummerzheim et al.* [1997] and *Germany et al.* [1997]. For the spacecraft, energies are plotted only where the flux is greater than 0.1 mW m^{-2}. The simulation appears to get significantly lower energies in the dayside oval.

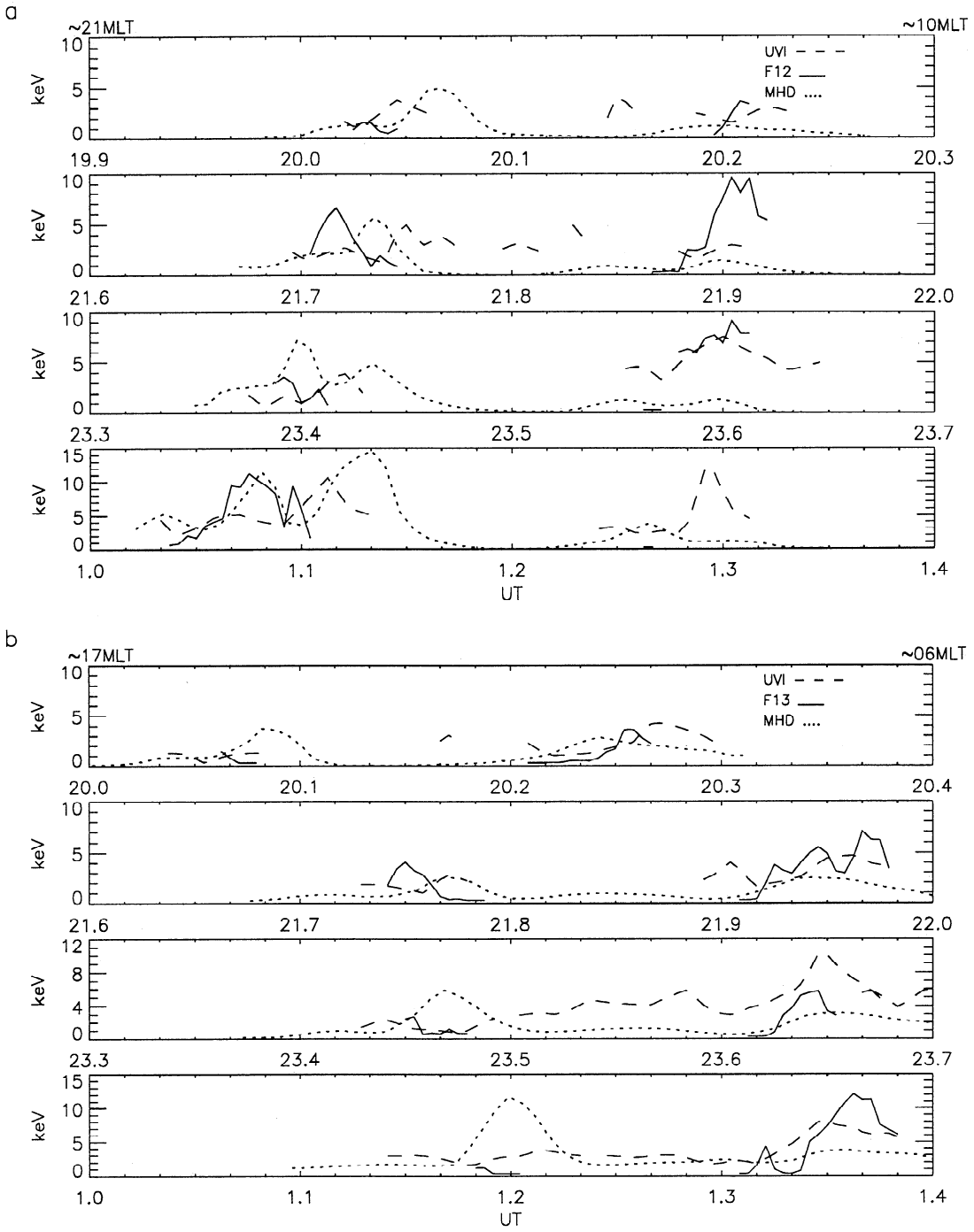

Figure 8. (a) The average energy of the precipitating electrons measured by F12 (solid), the UVI (dashed), and that given by the MHD simulation (dotted). The spacecraft data are plotted only where the measured flux is greater than 0.1 erg cm^{-3} s^{-1}. (b) The average energy for F13.

6. Overall Comparison

The MHD simulation began using the WIND solar wind measurements recorded at 1200 UT. The AMIE analysis using 5-min averages around of UVI images was begun around 1700 UT, so there were about five hours of MHD simulation before the comparison starts. However, we have made comparisons with the measurements of the Magnetic Field Experiment (MFE) [*Russell et al.*, 1995] during this period, and the data were reproduced fairly accurately [*Fedder et al.*, 1997]. Around 2020 UT a small substorm onset was observed with an auroral intensification in the premidnight sector. This substorm did not happen in the MHD simulation. A stronger substorm occurred after midnight, and this activity was reproduced fairly well.

It should be noted that once the MHD simulation began at 1200 UT no adjustments were made to the model or its parameters for the 14 hours of real time simulated apart from the solar wind inputs from WIND.

Figure 9a shows the total northern cross polar potential from the MHD simulation (solid) and the AMIE analysis (dashed) for the entire period during the AMIE run. The four vertical lines indicate the passage of the DMSP spacecraft which was discussed in detail in the last section. Figure 9b shows the ratio of the MHD result to the AMIE result. For this event the MHD cross polar potential is typically 30% higher during the first few hours of comparison. During the disturbed time after midnight, the ratio is more like 80%.

In previous published studies the total cross polar potential predicted by global MHD models has been much higher than AMIE values, sometimes by factors of 2 to 4 [*Fedder et al.*, 1998; *Raeder et al.*, 1998; *Winglee et al.*, 1997; *Lyons et al.*, 1996; *Lyons*, 1998; *Slinker et al.*, 1998; *Knipp et al.*, 1998]. The first five papers discussed the GEM challenge event of January 27-28, 1992; the last two papers modeled the magnetic storm which began on November 3, 1993. In both events the IMF was much larger than normal. The MHD simulation models usually agree with AMIE in the geometry of the convection patterns but with higher strengths.

In light of these earlier comparisons the closer agreement between the MHD and AMIE simulations for this event for which the strength of the IMF is typical, is encouraging.

The cause of the divergence of the results at highly disturbed times is not known. General theoretical arguments predict that the cross polar potential should scale linearly with the magnitude of the IMF [*Vasyliunas et al.*, 1982]. This scaling is consistent with our simulation, at least up to IMF magnitudes of 30 nT. Many data-based analyses of spacecraft measurements support a linear scaling at least up to 10 nT [*Boyle et al.*, 1997; *Reiff and Luhmann*, 1986, and references therein]. Though the IMF exceeds 10 nT several times a year, it is rare that a spacecraft is in a good observing position at the same time. *Reiff and Luhmann* [1986] discuss evidence for a saturation of polar cap potential and suggest possible mechanisms, but the question is still open. This is an important point to resolve since the most geoeffective events are those which are induced by a strong southward IMF.

Figure 9c shows the Joule heating of the northern polar cap predicted by the two models. The higher potentials in the MHD model lead to higher values.

Figure 9d shows the energy into the polar cap by precipitating electrons. This quantity is inferred from data of the Ultraviolet Imager (UVI) on POLAR [*Lummerzheim et al.*, 1997] and is used as part of the input to AMIE (dashed line). The result plotted here is higher in the quiet period than that reported by *Lummerzheim et al.* [1997] because in that calculation a threshold of 0.3 mW m^{-2} was used, whereas we used a threshold of zero. The dotted line shows hourly averages of estimated hemispheric auroral heating using precipitation measurements from the two NOAA [*Fuller-Rowell et al.*, 1987] and three DMSP spacecraft [*Rich et al.*, 1987]. The solid line is the MHD simulation result which greatly underestimates this source. Electron precipitation energy, as discussed in section 3, is used in the MHD model only as a means of estimating the ionospheric conductance through the *Robinson et al.* [1987] expression, equations (8) and (9). If the electron energy flux is viewed as a product of a average energy E times a particle number flux Ψ then the auroral Pedersen conductance depends mainly on E to the $3/2$ power and the square root of Ψ. The ratio of the Hall to Pedersen conductances depends only on E. Therefore, if we adjust the particle flux estimate in our model by a factor, f, and leave the average energy calculation alone, we will adjust the energy flux by f and the auroral conductances by the square root of f. Of course, this neglects the feedback of the adjustment in the time evolution of the system. As a result of the benchmarking of the MHD model with the UVI precipitation measurements for this event, we have used a value of f=2.56 which leads to an increase of 1.6 in the Pedersen and Hall conductances in our recent simulations. We also reran a section of this event with the improved flux estimate, and the results for the precipitation are shown as asterisks on Figure 9d. The result is still low compared to the UVI estimate, but the agreement is better and we will reevaluate the model in future runs.

For the time period of the rerun of this event, the general characteristics of the simulation did not change much. In particular, the simulation still did not pick up the premidnight auroral activation observed by the UVI at 2020 UT.

As noted above, increasing the flux estimate in the MHD model will increase the conductance, and to lowest order, decrease the polar cap potential according to eq. (1). This will bring the result closer to the AMIE potentials. However, the bulk of the potential drop usually occurs sunward of the terminator where the conductance is primarily due to ionization by sunlight.

Figure 9e shows the total downward field-aligned current flowing into the northern polar cap. (In the MHD simulation, the net hemispheric current is typically a few percent of the downward FAC.) The AMIE values and MHD values agree well, although there are differences in the geometric distribution as was pointed out in the last section.

Figure 9f shows the ratio of the polar cap potential drop to the total downward FAC giving a bulk resistance for the polar cap. Finally, Figure 9g gives the *AE*, *AL*, and *AU* calculated from the 52 stations between 55° and 76° magnetic latitude which were used in the AMIE analysis.

7. Conclusions

We have compared results in the northern polar ionosphere for a well-documented event from two models. One is an MHD global simulation model of the solar wind, the magnetosphere and the ionosphere which uses measured solar wind data as input. The other, AMIE, is a data assimilation model which incorporates many diverse ground- and space-based data sets. Moreover, the fundamental and derived ionospheric quanti-

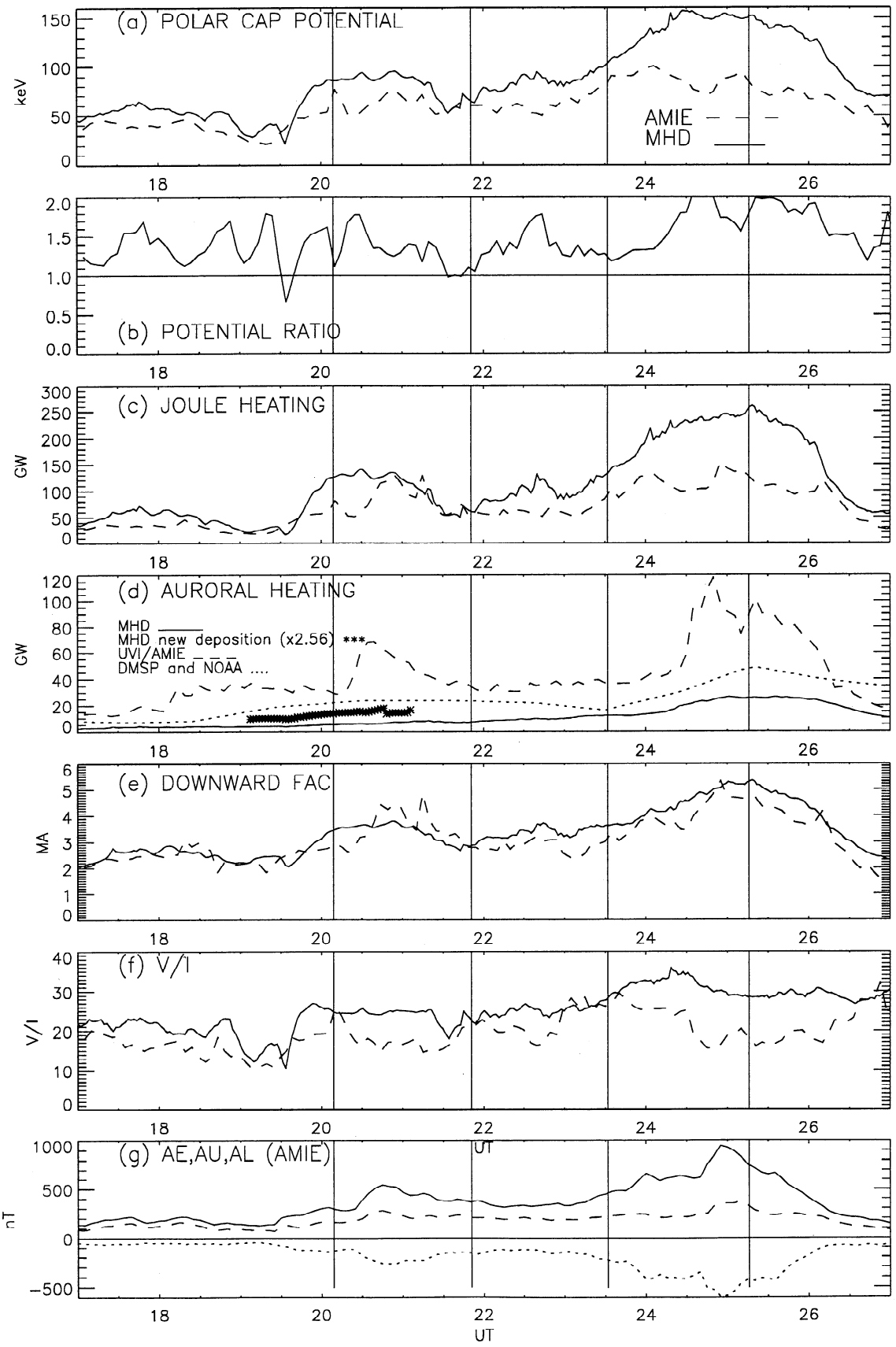
(a) POLAR CAP POTENTIAL
keV
AMIE
MHD
(b) POTENTIAL RATIO
(c) JOULE HEATING
GW
(d) AURORAL HEATING
MHD
MHD new deposition (x2.56)
UVI/AMIE
DMSP and NOAA
GW
(e) DOWNWARD FAC
MA
(f) V/I
V/I
(g) AE,AU,AL (AMIE)
nT
UT
18
20
22
24
26

ties differ between the two methods. For example, the field-aligned currents are a fundamental quantity in the MHD model formulation, but are derived for AMIE. There are many similarities in the results, giving confidence that both models are reproducing the behavior of the ionosphere in many respects.

The MHD model results did not diverge from the AMIE results as time progressed. AMIE is continually refreshed as new data is available while the MHD simulation uses only the measured solar wind information and is not otherwise adjusted as the simulation progresses. In fact, the MHD simulation actually began around 1200 UT nearly 5 hours before the AMIE comparisons were started. This shows the importance of the directly driven aspect of the solar wind on the Earth's magnetosphere/ionosphere system. It shows that even with no knowledge of the initial state of the system, given the solar wind parameters, one can have a pretty good idea of the current state of the system after several hours. It shows that if one could predict the solar wind as it reaches the Earth, one could predict the behavior of the magnetosphere and ionosphere reasonably well.

The MHD simulation underestimates the total auroral precipitation energy. This can and has been adjusted in the model. The ionosphere acts essentially as a boundary condition for the MHD simulation of the magnetosphere, so this adjustment is easy to implement. The model will be reevaluated in future event simulations.

The MHD simulation does not reproduce the intense morning precipitation. This effect is due, in part, to electron drifts which are not described in an ideal MHD formulation. To include this physics in the model would require some supplementary modification in the magnetospheric region which is not easily formulated. Various alternatives to address this issue are under consideration.

The MHD simulation predicts a somewhat higher total cross polar cap potential drop than AMIE, although the agreement is much better during the actual DMSP measurements of the field. This is in contrast to much greater differences seen under very disturbed conditions. The behavior of the polar cap potential under disturbed conditions is an important topic because of geoeffective considerations, and it is still an open question.

Acknowledgments. This study made use of the CEDAR Data Base at the National Center for Atmospheric Research which is supported by the NSF. We are also grateful to the following individuals and institutions for providing data for the analysis or for the AMIE simulation: R. Lepping (IMP 8 IMF data); A. Lazarus and K. Paularina (IMP 8 plasma data); G. K. Parks, M. J. Brittnacher, G. A. Germany, and J. F. Spann (POLAR UVI images); F. Rich (DMSP-F12 and F13 Ion Drift Meter data, electron precipitation data from F10, F12, and F13); D. Evans (electron precipitation data from NOAA 12 and NOAA 13);the Sondrestrom IS radar, which is supported by NSF; M. Ruohoniemi (Goose Bay and Kapuskasing SuperDARN HF radar data, which are operated by the Applied Physics Laboratory of the Johns Hopkins University with support from NSF and from NASA for Kapuskasing); G. Sofko (Saskatoon SuperDARN HF radar, which is operated by the University of Saskatchewan with support from the Natural Sciences and Engineering Research Council of Canada); J.-P. Villain (Stokkseyri SuperDARN HF radar data, which is operated by CNRS/LPCE and CNRS/CETP with support from the Inst. National des Sciences de l'Univers); M. Lester (CUTLASS SuperDARN HF radars at Hankasalmi and Pykkvibaer, which are operated by the Radio and Space Plasma Physics Group at the University of Leicester with support from the Particle Physics and Astronomy Council, and additional support from the Finnish Meteorological Institute and the Swedish Meteorological Institute). We are grateful for the following providers of magnetometer data: G. Rostoker and T. Hughes (CANOPUS, which is supported by the Canadian Space Agency); G. Van Beek (Energy Mines and Resources Canada); M. Engebretson and J. Hughes (MACCS); D. Milling (SAMNET); L. Morris (NGDC); H. Luehr (IMAGE); E. Friis-Christensen and T. Morretto (Danish Meteorological Institute); R. Sitar (MAGIC, University of Michigan); and the 210 Magnetic Meridian magnetometer chain. The 210 chain is managed by K. Yumoto and kept at the Solar-Terrestrial Environment Laboratory (STEL) at Nagoya University. The following individuals and institutions supported 210 ground magnetic observatories used in the AMIE study: Electronics Research Laboratory, K. J. W. Lynn, Australia; Biak Aerospace Observatory, Sukmadradjat, Indonesia; Birdsville Police Station, Australia; IPS Radio and Space Service, D. Cole, Australia; Kakioka Magnetic Observatory, S. Tsunomura, Japan; Dalby Agriculture College, Australia; University of Newcastle, B. J. Fraser and F. W. Menk, Australia; CSIRO Tropical Exosystems Research Center, Australia; Solar-Terrestrial Environment Laboratory (STEL), Japan; NOAA/Pacific Tsunami Warning Center, M. Blackford, USA; Katanning Research Station, Australia; Learmonth Solar Observatory, J. A. Kennewell; National Central University, J. K. Chao and Lunping Observatory, S.-W.

Figure 9. (a) The total potential drop across the northern polar cap from the MHD simulation (solid) and AMIE (dashed). The vertical lines are the DMSP overpass times. (b) The ratio of the MHD potential drop to that of AMIE. (c) The Joule heating rate from the MHD simulation (solid) and AMIE (dashed). (d) The heating rate due to precipitating electrons from the MHD simulation (solid) and the POLAR UVI measurements (dashed). Also shown is the rate estimated from NOAA 12,14 and DMSP F10,12,13 data (dotted). The asterisks indicate the result from a short rerun of the MHD simulation where the precipitation flux was multiplied by 2.56 as discussed in the text. (e) The total downward FAC from the MHD simulation (solid) and AMIE (dashed). (f) The ratio of the total potential drop to the total downward FAC for the MHD (solid) and AMIE (dashed). (g) The AE (solid), AU (dashed), and AL (dotted) calculated from 52 stations between 55° and 76° magnetic latitude.

Chen, Taiwan, Republic of China; Institute of Space Research and Radiowaves, E. F. Vershinin, V. V. Bogdaroj, and A. V. Buzevich, Russia; Coast and Geodetic Survey Deptartment, R. B. Feir, Phillippines; Tohoku University, T. Takahasi, Japan; Institute of Cosmophysical Research and Aeronomy, S. I. Solovyev and G. F. Krymsky, Russia; Institute of the Physics of Earth, V. A. Pilipenko, Russia; and Weipa North State School, Australia. WIND data were used courtesy of R.P. Lepping and K.W. Ogilvie. This work has been supported by the Office of Naval Research; and in part by a grant of HPC time from the DoD HPC Shared Resource Center, CEWES. JAF is partially supported by an NSF grant ATM-9613815 and NASA grant NAG5-4727. DL acknowledges support from NASA grant NAG5-7683 to the University of Alaska.

Janet G. Luhmann thanks Christophe Peymirat and Tuija Pulkkinen for their assistance in evaluating this paper.

References

Boyle, C. B., P. H. Reiff, and M. R. Hairston, Empirical polar cap potentials, *J. Geophys. Res., 102,* 111, 1997.

Chiu, Y. T., and J. M. Cornwall, Electrostatic model of a quict auroral arc, *J. Geophys. Res., 85,* 543, 1980.

Chiu, Y. T., A. L. Newman, and J. M. Cornwall, On the structures and mapping ofauroral electrostatic potentials, *J. Geophys. Res., 86,* 10,029, 1981.

Emery, B. A., et al., Assimilative mapping of ionospheric electrodynamics in the thermosphere-ionosphere general circulation model comparisons with global ionospheric and thermospheric observations during the GEM/SUNDIAL period of March 28-29, 1992, *J. Geophys. Res., , 101,* 26,681, 1996.

Fedder, J. A., and J. G. Lyon, The solar wind-magnetosphere-ionosphere current-voltage relationship, *Geophys. Res. Lett., 14,* 880, 1987.

Fedder, J. A., and J. G. Lyon, The Earth's magnetosphere is 165 R_E long: Self-consistent currents, convection, magnetospheric structure, and processes for northward interplanetary magnetic field, *J. Geophys. Res., 100,* 3623, 1995.

Fedder, J. A., J. G. Lyon, S. P. Slinker, and C. M. Mobarry, Topological structure of the magnetotail as a function of interplanetary magnetic field direction, *J. Geophys. Res., 100,* 3613, 1995a.

Fedder, J. A., S. P. Slinker, J. G. Lyon, and R. D. Elphinstone, Global numerical simulation of the growth phase and the expansion onset for a substorm observed by Viking, *J. Geophys. Res., 100,* 19,083, 1995b.

Fedder, J. A., S. P. Slinker, J. G. Lyon, C. T. Russell, F. R. Fenrich, and J. G. Luhmann, A first comparison of POLAR magnetic field measurements and magnetohydrodynamic simulation results for field-aligned currents, *Geophys. Res. Lett., 24,* 2491, 1997.

Fedder, J. A., S. P. Slinker, and J. G. Lyon, A comparison of global simulation results to data for the January 27-28, 1992, Geospace Environment Modeling challenge event, *J. Geophys. Res., 103,* 14,799, 1998.

Fuller-Rowell, T. J. and D. S. Evans, Height-integrated Pedersen and Hall conductivity patterns inferred from the TIROS-NOAA satellite data, *J. Geophys. Res., 92,* 7606, 1987.

Germany, G. A., G. K. Parks, M. Brittnacher, J. Cumnock, D. Lummerzheim, J. F. Spann, L. Chen, P. G. Richards, and F. J. Rich, Remote determination of auroral energy characterstics during substorm activity, *Geophys. Res. Lett., 24,* 995, 1997.

Knipp, D. J., et al., An overview of the early November 1993 geomagnetic storm, *J. Geophys. Res., 103,* 26,197, 1998.

Lepping, R. P., et al., The Wind magnetic field investigation, *Space Sci. Rev., 71,* 207, 1995.

Lummerzheim, D., M. H. Rees, J. D. Craven, and L. A. Frank, Ionospheric conductances derived from DE-1 auroral images, *J. Atmos. Terr. Phys., 53,* 281, 1991.

Lummerzheim, D., M. Brittnacher, D. Evans, G. A. Germany, G. K. Parks, M. H. Rees, and J. F. Spann, High time resolution study of the hemispheric power carried by energetic electrons into the ionosphere during the May 19/20, 1996 auroral activity, *Geophys. Res. Lett., 24,* 987, 1997.

Lyons, L. R., The Geospace Environment Modeling grand challenge, *J. Geophys. Res., 103,* 14,781, 1998.

Lyons, L. R., G. Lu, O. de la Beaujardice, and F. J. Rich, Synoptic maps of polar caps for stable IMF intervals during January 1992 GEM campaign, *J. Geophys. Res., 101,* 17,121, 1996.

Mobarry, C. M., J. A. Fedder, and J. G. Lyon, Equatorial plasma convection from global simulations of the Earth's magnetosphere, *J. Geophys. Res., 101,* 7859, 1996.

Ogilvie, K. W., et al., SWE, A comprehensive plasma instrument for the Wind spacecraft, *Space Sci. Rev., 71,* 55, 1995.

Orens, J. H., and J. A. Fedder, The effects of geomagnetic field-aligned potential differences on precipitating magnetospheric particles, *NRL Memo. Rep. 3573,* 1978.

Raeder, J., J. Berchem, and M. Ashour-Abdalla, The geospace environment modeling grand challenge: Results from a global geospace circulation model, *J. Geophys. Res., 103* 14,787, 1998.

Rees, M. H., D. Lummerzheim, and R. G. Roble, Modeling of the atmosphere-magnetosphere-ionosphere system (MAMI), *Space Sci. Rev., 71,* 691, 1995.

Reiff, P. H., and J. G. Luhmann, Solar wind control of the polar cap voltage, in *Solar Wind-Magnetosphere Coupling,* edited by Y. Kamide and J. Slavin, p. 453, Terra Sci., Tokyo, 1986.

Rich, F. J., M. S. Gussenhoven, and M. E. Greenspan, Using simultaneous particle and field observations on a low altitude satellite to estimate Joule heat energy flow into the high latitude ionosphere, *Ann. Geophys., 5,* 527, 1987.

Richmond, A. D., Assimilative mapping of ionospheric electrodynamics, *Adv. Space Res., 12*(6), 59, 1992.

Richmond, A. D., and Y. Kamide, I. Mapping electrodynamic features of the high-latitude ionosphere from localized observations: Technique, *J. Geophys. Res., 93,* 5741, 1988.

Robinson, R. M., R. R. Vondrak, K. Miller, T. Dabbs, and D. Hardy, On calculating ionospheric conductances from the flux and energy of precipitating electrons, *J. Geophys. Res., 92,* 2565, 1987.

Russell, C. T., R. C. Snare, J. D. Means, D. Pierce, D. Dearborn, M. Larson, G. Barr, and G. Le, The GGS Polar magnetic field investigation, *Space Sci. Rev., 71,* 563, 1995.

Slinker, S. P., J. A. Fedder, J. Chen, and J. G. Lyon, Global MHD simulation of the magnetosphere and ionosphere for 1930-2330 UT on November 3, 1993, *J. Geophys. Res., 103,* 26,243, 1998.

Torr, M. R., et al., A far ultraviolet imager for the International Solar-Terrestrial Physics Mission, *Space Sci. Rev., 71,* 329, 1995.

Vasyliunas, V., J. R. Kan, G. L. Siscoe, and S.-I. Akasufu, Scaling relations governing magnetospheric energy transfer, *Planet. Space Sci., 30,* 359, 1982.

Weimer, D R. Models of high-latitude electric potentials derived with a least error fit of spherical harmonic coefficients, *J. Geophys. Res., 100,* 19,595, 1995.

Weimer, D.R., A flexible, IMF dependent model of high-

latitude electric potentials having "space weather" applications, *Geophys. Res. Lett., 23,* 2549, 1996.

Winglee, R. M., V. O. Papitashvili, and D. R. Weimer, Comparison of the high-latitude ionospheric electrodynamics inferred from global simulations and semiempirical models for the January 1992 GEM campaign, *J. Geophys. Res., 102,* 26,961, 1997.

K. B. Baker, Applied Physics Laboratory, Johns Hopkins University, Laurel, MD 20723. (kile_baker@jhuapl.edu)

B. A. Emery, High Altitude Observatory, National Center for Atmospheric Research, Boulder, CO 80307. (emery@ucar.edu)

J. A. Fedder, and S. P. Slinker, Code 6794, Plasma Physics Division, Naval Research Laboratory, Washington, DC 20375. (slinker@ppdu.nrl.navy.mil)

D. Lummerzheim, Geophysical Institute, University of Alaska, Fairbanks, AK 99775. (lumm@gi.alaska.edu)

J. G. Lyon, Department of Physics, Dartmouth College, Hanover, NH 03755. (lyon@tinman.dartmouth.edu)

F. J. Rich, Space Vehicles Directorate, Air Force Research Laboratory, Hanscom AFB, MA 01731. (rich@plh.af.mil)

(Received May 6, 1999; revised August 3, 1999; accepted August 29, 1999.)